Toward an optimum design of an amorphous silicon photovoltaic/thermal system: simulation and experiments

Xiao Ren[a], Jing Li[b,*], Weixin Liu[c], Chuanyong Zhu[a], Gang Pei[c], Liang Gong[a,*]

[a] *College of New Energy, China University of Petroleum (East China), Qingdao 266580, China*

[b] *Research Center for Sustainable Energy Technologies, Energy and Environment Institute, University of Hull, Hull, HU6 7RX, UK*

[c] *Department of Thermal Science and Energy Engineering, University of Science and Technology of China, 96 Jinzhai Road, Hefei 230026, China*

[*]Corresponding author. Tel. /Fax: Jing.li@hull.ac.uk; lgong@upc.edu.cn

Abstract:

Amorphous silicon photovoltaic/thermal (a-Si- PV/T) technology is promising due to the low power temperature coefficient, thin-film property, thermal annealing effect of the solar cells, and high conversion efficiency in summer. The design of a-Si-PV/T system is influenced by a number of thermodynamic, structural, and external parameters. Parametric analysis is useful for a good design of the system. A dynamic distributed parameter model is built and verified in this paper. Outdoor tests are carried out. The impacts of operating temperature, mass flow rate, cover ratio of solar cells, heat transfer area, and frame shadow ratio on its performance are theoretically and experimentally investigated. The results indicate that seven or eight copper tubes are suitable to achieve a high overall efficiency of the a-Si-PV/T. The frame and tilt angle shall avoid a shadow ratio of more than 8.3% during operation. The difference between power outputs at operating temperatures of 35 °C and 55 °C in the first month is about 0.21 % while it drops to less than 0.1% in the twelfth month. Compared with conventional PVT systems, the a-Si-PV/T benefits from a higher design temperature with a minor

efficiency decrement.

Keywords: amorphous silicon cell, photovoltaic thermal system, parametric analysis, distributed parameter model, frame shadow

1. Introduction

Hybrid photovoltaic/thermal (PV/T) technology is the integration of photothermal (PT) and photovoltaic (PV) modules with higher solar energy utilization efficiency and has great potential in the field of combined heat and power. The mainstream PV material of PV/T systems is usually crystalline silicon (c-Si) cells. However, several drawbacks of c-Si cells have limited the development of PV/T technology, such as the electricity loss due to the high power temperature coefficients (−0.4 %/°C to −0.5 %/°C) and the technical problem of interruption due to the large thermal stresses [1]. Compared with c-Si-PV/T, the application of amorphous silicon (a-Si) cells in PV/T systems has received increasing attention. Many superior characteristics of a-Si cells, such as low power temperature coefficient, thin-film property, low thermal resistance, thermal annealing effect, and high conversion efficiency in summer, make them distinctive in the PV/T application [2, 3]. The low-temperature coefficient (–0.1 %/°C to –0.2 %/°C or even positive) can avoid substantial power loss at high temperatures [4]. The a-Si cells with thin film and flexible properties can use metal as the substrates and exhibit lower thermal resistance compared with c-Si cells. They can overcome the technical problem of interruption in c-Si PVT at periodically fluctuating temperatures [5]. Besides, the electrical property of a-Si cells varies seasonally[6, 7], i.e. higher in summer and lower in winter, which is the opposite of c-Si cells, and this phenomenon is attributed to the spectral effects, which are related to changes in the spectral content of the sunlight during the year [8]. Thus, more electricity can be obtained in summer when there is less demand for heat. However, the Staebler–Wronski (SW) effect

has limited the development of a-Si cells, which is related to the light-induced degradation of electrical performance and the creation of defect states. Studies have shown that high temperature can reduce this SW effect [9], and the temperature inside the PV/T is higher than the ambient temperature, which is beneficial to a-Si cells [10]. A novel a-Si-PV/T system has been recently built by the authors [11]. This is the first attempt to use the a-Si cells with stainless steel as a substrate in a real PV/T system. Its feasibility at medium operating temperatures has been demonstrated [12].

As a newly developed system, an insight into the influence of the parameters is needed. The properties of the a-Si-PV/T system are expected to be affected by a number of thermodynamic, structural, and external parameters. At present, numerous studies have been conducted on parametric influences in the c-Si-PV/T systems. The influences of operating temperature [13], mass flow rate of heat transfer fluid [14], cover ratio of solar cells [15], number of copper tubes [16], and shadow ratio [17], etc., have been assessed. However, there is a limited parametric analysis of the a-Si-PV/T collectors. A few theoretical studies on the effect of a-Si intrinsic layer thickness [18], dispatch strategies [19], and heat treatments [20] on the electrical property of the a-Si cells. The influences of shadow, long-term operating temperature, heat transfer area, etc. have not been discussed. Notably, the conclusions drawn from the existing works on c-Si-PV/T systems may not be applicable to a-Si-PV/T systems. Some reasons are provided as follows.

First, the temperature is one of the most meaningful parameters of PV/T systems. The temperature effect on c-Si-PV/T is relatively simple, and its electrical efficiency decreased linearly as the c-Si cell temperature rises [21]. The impact on the a-Si cells, by contrast, is complicated. It is subjected to light-induced metastable changes in the properties of a-Si cells and depends on time [22]. On the one hand, the performance is degraded rapidly in the first 6 months and becomes relatively stable afterward. On

the other hand, a higher operating temperature can facilitate better thermal annealing, leading to higher electrical efficiency at the degraded steady state (DSS) [23]. To sum up, the power output affected by operating temperature is difficult to predict.

Second, the frame shadow is an important factor affecting the electrical performance in the PV/T system. To reduce heat loss and improve the overall efficiency, an air layer is generally set between the photovoltaic (PV) module and glass cover in most PVT systems[24]. However, when the sunlight is obliquely incident in the morning and evening, the frame border will cast shadows on the PV module near the frame. Instead of generating electricity, the shaded cells can consume the power generated by the non-shaded cells, and the generated hot spots may cause irreversible damage to the PV cell [25]. The effect of frame shadow on c-Si-PV/T systems has been investigated through experiments and simulations [26, 27]. Usually, the electrical efficiency in a series circuit first drops fast and then remains unchanged, while in a parallel circuit the electrical efficiency declined linearly as the shadow increased. The electrical efficiency decreases by 2.6% (normal efficiency, 13.0%) under frame shadow in the worst case of Hefei [28]. The effect of shadow is related to the I-V characteristic of the solar cells. To the authors' knowledge, there is no research on the influence of frame shadow on the PV/T system employing a-Si cells.

Third, the thin-film a-Si cells with stainless steel as the substrate offer high thermal conductivity. The heat transfer performance of a-Si-PV/T collectors is distinct from that of a c-Si-PV/T, resulting in different parametric optimizations. For example, it might be unnecessary to use a large number of copper tubes to carry away the heat collected by the collectors.

In this paper, parametric influences on the PV/T system employing a-Si cells are investigated theoretically and experimentally. A distributed parameter model of transient heat transfer is established

and validated by experiments. Internal views of the heat transfer and power generation are provided, and the non-uniform temperature profiles on the PV/T components are illustrated. Focus is put on the PV/T performance at different operating temperatures and shadow ratios. Besides, the effects of the number of copper tubes, mass flow rate of water, and cover ratio of solar cells are examined.

Nomenclature

a-Si	amorphous silicon
A	area, m^2
B	temperature coefficient, K^{-1}
c	specific heat capacity, J/kg·K
C	perimeter, m
c-Si	crystalline silicon
d	thickness, m
D	diameter, m
$\dot{E}x$	Exergy, J
G	solar irradiation, W/m^2
h	heat transfer coefficient, $W/m^2 \cdot K$
H	total solar irradiance MJ/m^2
I	current, A
K	extinction coefficient, m^{-1}
L	length, m
m	mass flow rate, kg/s
M	mass, kg
MRE	mean relative error
n	refractive index
Nu	Nusselt number
P	electrical gain, J
PV/T	photovoltaic/thermal
Q	energy, J, MJ
R	thermal resistance, K/W
Ra	Raleigh number
RE	relative error
t	time, s
T	temperature, K
U	voltage, V

Greek letters

α	absorptivity
β	slope angle of collector, °
θ	incidence angle, °
ϕ	latitude, °
ω	hour angle of the sun, °
γ	surface azimuth angle, °
δ	declination angle of the sun, °
ε	emissivity
η	efficiency
ξ	cover ratio
λ	thermal conduction, W/m·K
γ	azimuth angle, °
ρ	density, kg/m^3
ρ_d	reflection of glass cover,-
σ	Stefan-Boltzman constant, $W/m^2 \cdot K^4$
τ	transmittance
$(\tau\alpha)$	transmittance-absorptance product
ω	solar hour angle, °

Subscripts

a	ambient, air
ad	adhesive layer
b	absorber plate
bt	welding layer
c	collector
d	day
e	sky
ex	exergy
exp	experiment
g	glass
il	insulation layer
ij	a single controller
in	inlet of collector
mp	maximum power
out	outlet of collector
pv	PV module
pv,s	shaded PV module
pvt	PV/T
ref	standard test condition
sim	simulation
sun	solar
t	copper tube
th	thermal
tank	water-storage tank
TPT	black TPT
w	water
wt	water in the tank
w,i	initial temperature
w,f	final temperature

2. Methodology

The parametric analysis is carried out through two methods of experiment and simulation. For instance, the influence of frame shadow is investigated experimentally. Due to the manufacturing costs and processing difficulties, some parametric conditions, such as the number of copper tubes and cover ratio are analyzed through the simulation. Besides, the effects of operating temperature and mass flow rate of water are also examined through simulation. The reliability verification of the simulation model is validated by outdoor experiments.

2.1 Experimental method

The experiment system for the a-Si-PV/T collector is constructed in Hefei, China with a longitude of 117.15° E and latitude of 34.27° N. Seven copper tubes are welded on the back of the aluminum plate. Fifteen a-Si cells are connected in series (no diode connection between the a-Si cells) and laminated on the aluminum plate. The parameters of the a-Si-PV/T collector and the PV characteristics of an a-Si cell at standard test conditions are shown in Table 1. The actual setup and schematic diagram of the a-Si-PV/T system are shown in Fig. 1 and Fig. 2. The collector is installed southward with a slope angle of 30°. The circulation pump between the water-storage tank (with a capacity of 80 L) and the collector is used to circulate the working medium (water). Five thermocouples (Type T) are arranged evenly in the water-storage tank from the top to the bottom. During the processing of the collector, thermocouples (Type T) are arranged on the back of the absorber plate to measure its temperature. To accurately calculate the thermal efficiency, a water flowmeter is employed to measure the mass flow rate of the water. The global solar radiation received on the collector surface is measured by a radiometer and its installation angle is the same as that of the collector. The maximum power point current and voltage are measured by a maximum power point tracking solar charge controller.

The platinum resistance with an uncertainty of ± 0.1 °C is used to measure the temperatures of the inlet and outlet water. The measurement accuracy of related measuring instruments is shown in Table 2. In this study, full-day experiments are conducted to verify the accuracy of the mathematical model. The measurement data are recorded by a computer data-acquisition system (Agilent Bench Link Date Logger).

Table 1 Parameters of the a-Si-PV/T collector.

Parameters	Value	Parameters	Value
An a-Si cell area	356mm×239mm	Thickness of glass cover	3.2 mm
Absorber plate area	1950mm×950mm	Thickness of air gap	26 mm
Lenth of copper tube	1900 mm	Thickness of a-Si cell	1.5 mm
Outer diameter of copper tube	8 mm	Thickness of absorber plate	1.16 mm
Density of glass cover	2500 kg/m^2	Thickness of insulating plate	36 mm
Density of a-Si cell	1700 kg/m^2	Number of a-Si cells	15
Density of absorber plate	2702 kg/m^2	Number of copper tubes	7
Density of copper tube	8933 kg/m^2	Open circuit voltage of an a-Si cell	2.1V
Specific heat capacity of glass cover	835 J/kg·K	Short circuit current of an a-Si cell	5.1A
Specific heat capacity of a-Si cell	500 J/kg·K	Voltage at max power of an a-Si cell	1.6V
Specific heat capacity of absorber plate	917 J/kg·K	Current at max power of an a-Si cell	4.1A
Specific heat capacity of copper tube	385 J/kg·K	Absorptivity of black TPT	0.95
Thermal conduction of glass cover	1.4 W/m·K	Absorptivity of a-Si cell	0.757
Thermal conduction of a-Si cell	20 W/m·K	Fill factor of an a-Si cell	61%
Thermal conduction of absorber plate	238 W/m·K	Power temperature coefficient	-0.2%/°C
Thermal conduction of copper tube	397 W/m·K		

Fig. 1. Actual setup of the a-Si-PV/T system test rig.

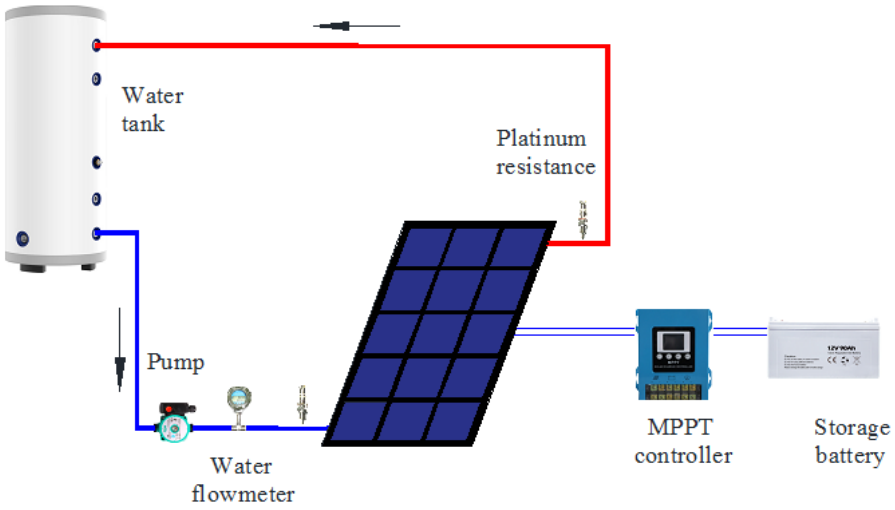

Fig. 2. Schematic diagram of the a-Si-PV/T system test rig.

Table 2 Measurement accuracy and type of related measuring instruments.

Instruments	Types	Measurement accuracy
Thermocouple	Type T	±0.5°C
Thermal resistance	Pt 100	±0.1 °C
Radiometer	TBQ-2	±2%
Flowmeter	LWGY	±5%
Current sensor	HKK-13-I	±0.1%

Due to the lack of a widely applicable mathematical model of frame shadow, the influence of frame shadow is investigated experimentally. Experiments are carried out and the ratio of the shaded area to the total area of PV module is set to 0%, 8.3%, 16.7%, and 25.0% as shown in Fig. 3. The shadow is shaded by the opaque baffles over PV module. These experiments are performed in a short period with little change in solar irradiance. In addition, to avoid the unreliability of a single experiment, the authors conduct two groups of experiments with the same boundary conditions. The data, such as open-circuit voltage, short-circuit current, maximum power point voltage and current, are measured by the I-V curve tester (I-V 400, HT Italia).

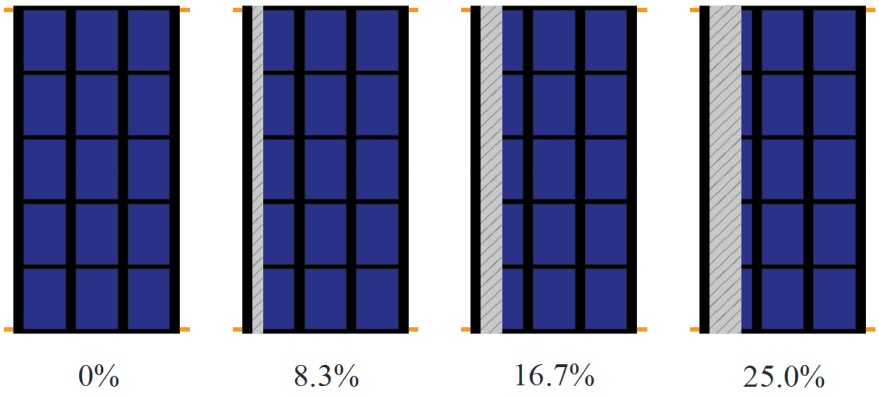

Fig. 3. Different ratios of the shaded area to the total area of PV module.

2.2 Simulation method

A distributed parameter model is developed for prediction and optimization under different parametric conditions, such as inlet water temperature, mass flow rate, cover ratio, and number of copper tubes. As shown in Fig. 4, the heat transfer process inside the a-Si-PV/T collector is shown in the cross section. The display area of the temperature distributions of the PV module and the absorber plate in Section 3 is also shown in Fig. 4. The two-dimensional discrete nodes (i×j =51×11) of the PV module and absorber plate are shown in Fig. 5. For the copper tube and the water in it, 49×1 nodes are established for grid discretization. The detailed mathematical model is given in Appendix. To solve the model and predict the performance of the a-Si-PV/T system, a numerical simulation program is written in MATLAB. The daily and annual flow charts of the calculation process for the a-Si-PV/T system are shown in Fig. 6.

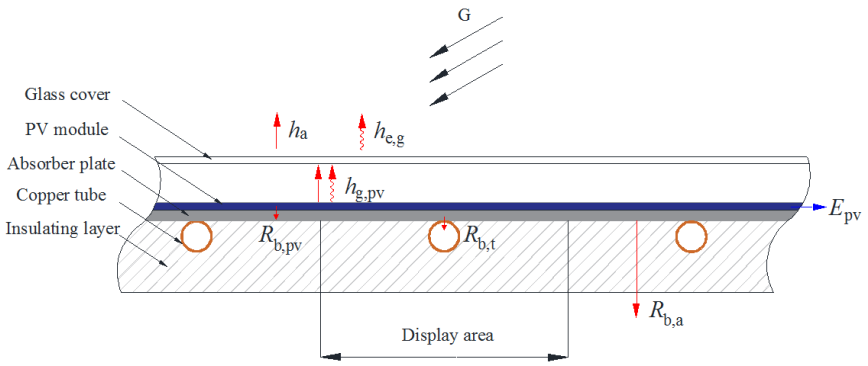

Fig. 4. Cross section and heat transfer process of the a-Si-PV/T collector.

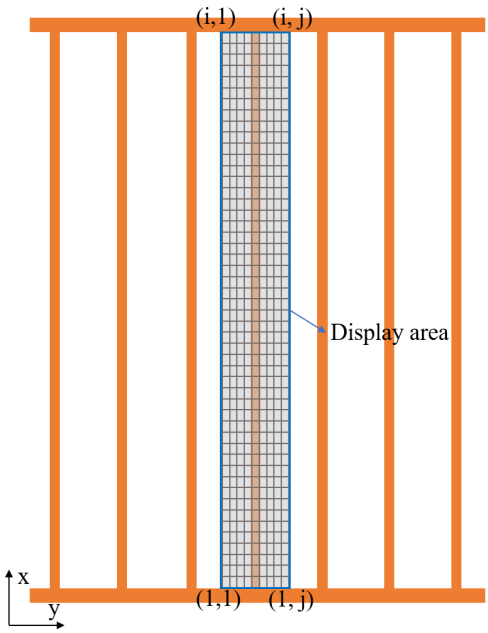

Fig. 5. Differential grid partition and display area of PV module and absorber plate.

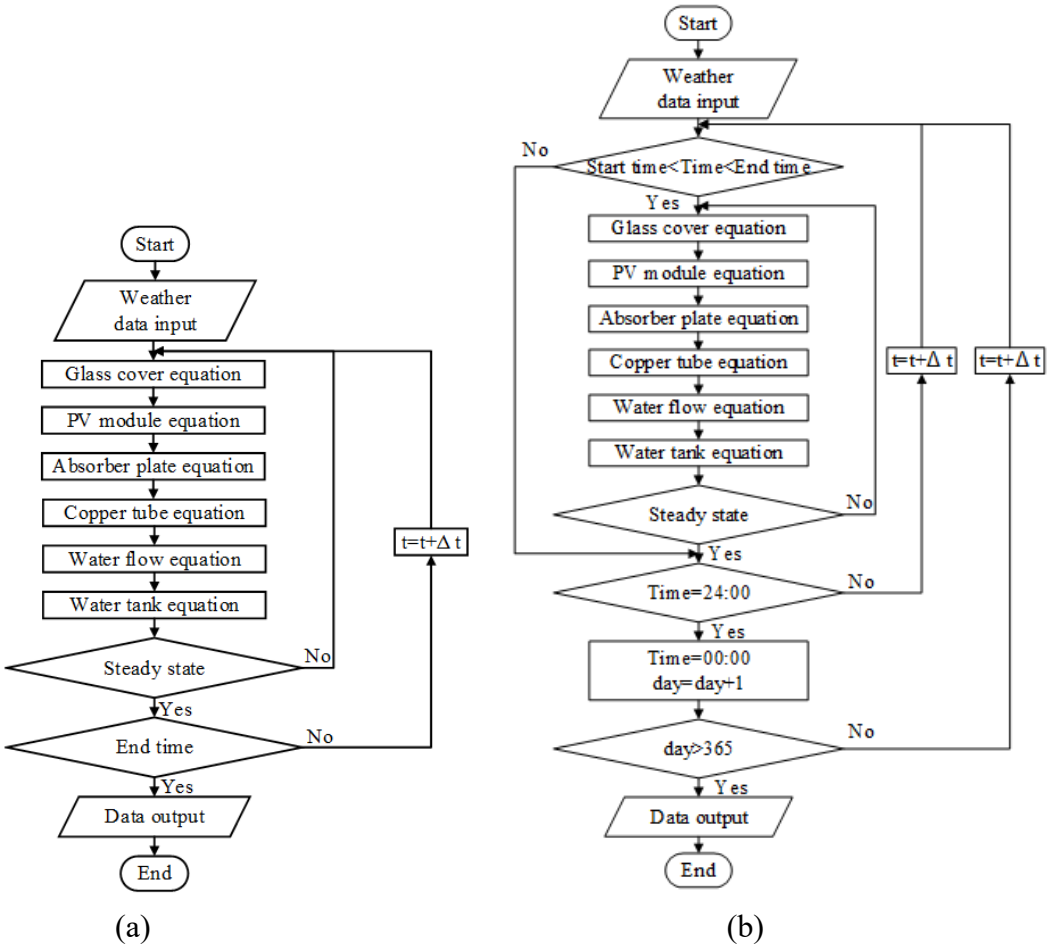

Fig. 6. Daily and annual flow charts of the calculation process for the a-Si-PV/T system.

3. Results and discussion

3.1 Experimental validation of the mathematical models

A full day experiment was conducted from 8:30 to 15:00 on December 10, 2017. The mass flow rate of the circulating water was set to approximately 0.044 kg/s. The actual measured ambient parameters during a full-day experiment are given in Fig. 7. The daily average ambient temperature is 10.3 °C and the maximum solar irradiance is 787.57 W/m^2 at 12:03. Simulation is conducted based on the mathematical model and ambient parameters.

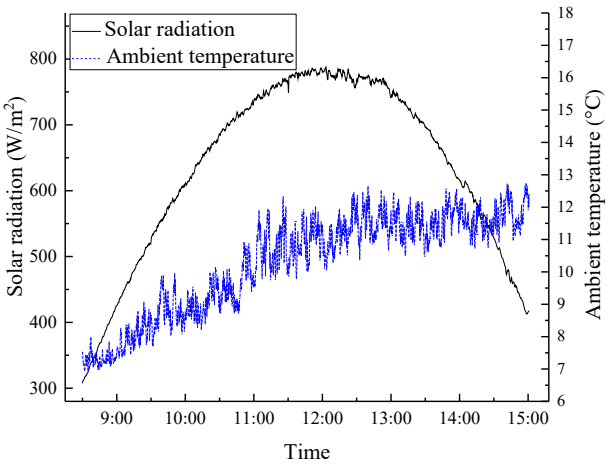

Fig. 7. Variations of ambient temperature and solar irradiance on December 10, 2017.

As shown in Fig. 8 and Fig. 9, the results indicate that the simulated temperatures of aluminum plate, water in the tank, inlet, and outlet water are in good agreement with the experimental ones. The experimental and simulation results of the final water temperatures in the tank are 43.4 °C and 43.8 °C with the same initial water temperature of 10.8 °C. The REs of the water temperature in the tank are within −2.0% to 0.9%. The MREs of the average temperatures of the aluminum plate, water in the tank, inlet, and outlet water are only 1.8%, 0.9%, 1.7%, and 1.3%, respectively. These outcomes prove that the simulation is in approximate accordance with the experiment in a whole day.

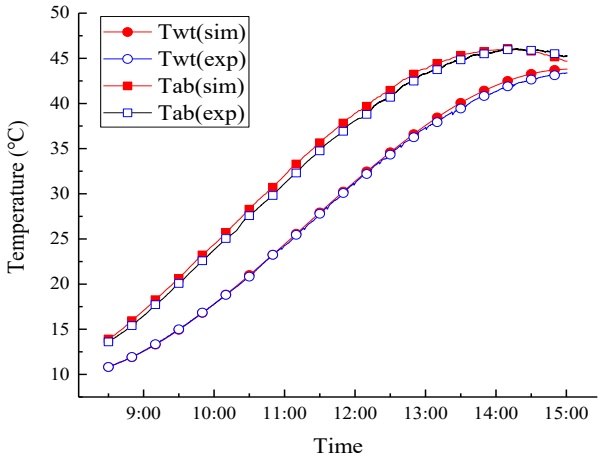

Fig. 8. Simulation and experimental results of the average temperatures of the aluminum plate and the water in the tank.

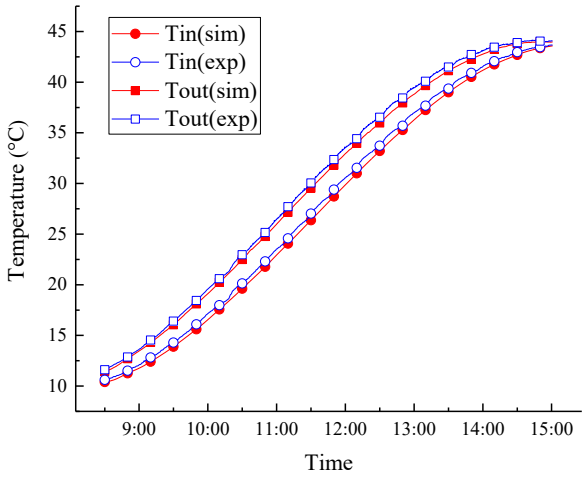

Fig. 9. Simulation and experimental results of the water temperatures at the inlet and outlet.

As shown in Fig. 10, the simulation and experimental results of the instantaneous thermal efficiency and heat gain of the a-Si-PV/T collector are in good agreement and follow the same trend with a minor difference. The MRE of the instantaneous thermal efficiency and heat gain is only 2.5%, and the value of RE fluctuates between 4.88% and 9.69%. The trend of the heat gain of the system is highly correlated with the variation of solar irradiance. The instantaneous thermal efficiency is high in the morning, and the experimental and simulation results of the maximum instantaneous thermal efficiency are 42.54% and 43.73%. In the afternoon, as the temperature of the water in the tank gradually increases and the solar irradiance reduces, the heat loss between the collector and

surrounding air increases, resulting in a downward trend in thermal efficiency.

The simulation and experimental results of the electrical gain and efficiency are compared in Fig. 11. Since the effect of the frame shadow is not considered in this mathematical model, the tested electrical efficiency is much lower than the simulated one before 9:00. In a PV/T system, a frame shadow can significantly influence the performance of the PV module [26]. The simulation and experimental results of the average electrical efficiencies are both 6.1% without shadow effect from 10:00 to 14:00. In the meantime, as the temperature increases, the electrical efficiency shows a slight drop, and the power temperature coefficient of the a-Si cells can be calculated as −0.2 %/ °C in this short-time test. The MRE of electrical efficiency and electrical gain in a full day test is 3.2%. A good agreement is observed between the experimental results and simulation results in most of the day, but the bias is larger in the morning.

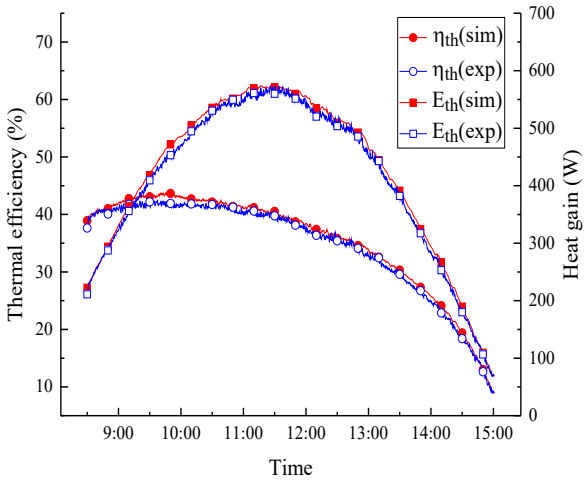

Fig. 10. Simulation and experimental results of the instantaneous thermal efficiency and heat gain.

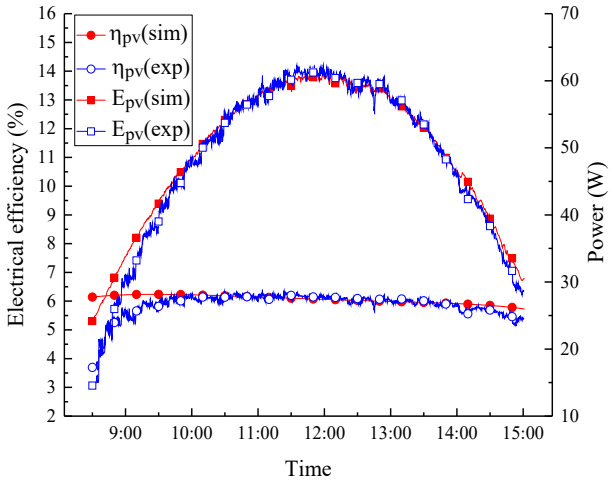

Fig. 11. Simulation and experimental results of instantaneous electrical gain and efficiency.

The simulation and experimental results of the exergy efficiency regarding the heat and electrical gain are shown in Fig. 12. In terms of the exergy efficiency of heat gain, a trend different from thermal efficiency is found. The exergy efficiency increases first and decreases afterward with the water temperature increasing from 10.8 °C to 43.4 °C, and the peak of exergy efficiency occurs around 13:00 with a value of 3.11% when the inlet water temperature is 35.3 °C. In addition, the exergy efficiency of electrical gain shows the same trend as electrical efficiency, but the values of the former are slightly higher than that of the latter since the exergy content of solar irradiance is lower than the solar irradiance.

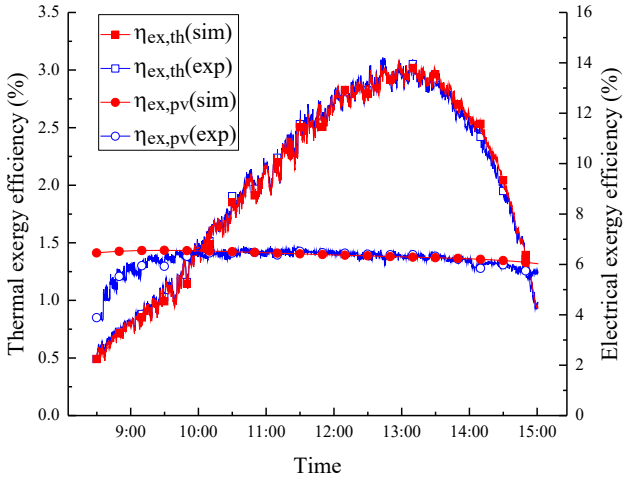

Fig. 12. Simulation and experimental results of exergy efficiency.

The daily simulated performance is consistent with the experimental performance, as shown in Table 3. The experimental results of the daily average thermal efficiency, electrical efficiency, and overall efficiency are 39.63%, 5.87%, and 50.27%, whilst the REs of the three parameters are only −1.2%, −3.3%, and −1.7%, respectively.

Table 3 Comparison of the results of the full-day experiment and simulation.

Result	H (MJ/m^2)	$\overline{T_{w,i}}$ (°C)	$\overline{T_{w,f}}$ (°C)	$\eta_{th,a}$ (%)	$\eta_{pv,a}$ (%)	$\eta_{pvt,a}$ (%)	$\eta_{ex,th,a}$ (%)	$\eta_{ex,pv,a}$ (%)	$\eta_{ex,pvt,a}$ (%)
Experiment	14.92	10.8	43.4	39.63	5.87	50.27	2.33	6.25	6.64
Simulation			43.8	40.11	6.07	51.11	2.37	6.38	6.76
RE				−1.2	−3.3	−1.7	−1.7	−2.0	−1.8

Similarly, the simulation and experimental results at different operating temperatures (60 °C, 70 °C, and 80 °C) are compared. As shown in Table 4. The MRE of the thermal and electrical efficiency is between 2.54% to 4.99% and between 1.10% and 2.78%, respectively. The accuracy and reliability of the numerical simulation are proved. Therefore, the established mathematical model can be used to accurately simulate and predict the property of the a-Si-PV/T system.

Table 4 MREs between the simulation and experimental results at different operating temperatures.

T_{in}(°C)	Date		$\eta_{th,a}$	$\eta_{pv,a}$
60	2018.11.27	Experiment	18.09%	5.30%
		Simulation	18.49%	5.36%
		MRE	3.27%	2.20%
70	2019.03.07	Experiment	22.00%	5.10%
		Simulation	21.84%	5.08%
		MRE	2.54%	1.10%
80	2019.03.10	Experiment	13.87%	4.81%
		Simulation	14.00%	4.90%
		MRE	4.99%	1.96%

In addition, the uncertainties of the measurements are calculated. The average relative uncertainties of the instantaneous thermal efficiency, daily average thermal and electrical efficiency are ±9.82%,

±2.95%, and ±2.00%. Thus, it is proved that the measuring instruments can guarantee the accuracy of the experimental results.

3.2 Parametric analysis

The influences of the key parameters can be predicted by the models established in Section 2 and validated in Section 3.1, with the exception of frame shadow. On the one hand, the impact of frame shadow on the a-Si-PV/T performance is of interest. Shading analysis is an essential step in the phase of the system analysis and no relevant work on a-Si-PV/T has been investigated in the literature. On the other hand, unlike well-developed heat transfer models, an accurate model for partially shaded PV systems is lacking [29]. The shading analyzers using software and hardware units generally use real-time data [30]. At present test data on a-Si-PV/T are rare. In this regard, an experimental approach to the impact assessment of frame shadow is adopted, while the influences of PV cover ratio, number of copper tubes, operating temperature, and mass flow rate are simulated.

3.2.1 Frame shadow

It is found that the tested electrical efficiency is much lower than the simulated ones before 9:00, which may be due to the influence of frame shadow. Therefore, the authors investigate the effect of the frame shadow on the a-Si-PV/T systems. Two groups of experiments are carried out and the ratio of the shaded area to the total area of the PV module is set to 0%, 8.3%, 16.7%, and 25.0%.

As shown in Fig. 13 and Table 5, the results of the two groups are coincident with the other. As the shaded area increases, the electrical efficiency, open-circuit voltage and short-circuit current gradually decrease. Among them, the frame shadow has less influence on the open-circuit voltage. As the area ratio of the shadow to the total PV module increases from 0 to 25%, the open-circuit voltage only decreases by less than 1V. When the ratios are 0%, 8.3%, 16.7% and 25.0%, the electrical efficiencies

each are 5.36%, 5.31%, 4.42% and 2.78% in test 1. When the shadow ratio increases from 0% to 8.3%, it has little effect on electrical performance, but when the shadow ratio continues to increase, the electrical efficiency decreases significantly. One can observe that the effect of frame shadow on the a-Si cells is different from that on the c-Si cells. For example, Wang et al. [26] investigated the effect of frame shadow on c-Si cells of PV/T collector by simulation and found that the electrical efficiency of the series circuit drops rapidly at first, and then remains unchanged. When the area ratio of shadow to PV cells increases from 0% to 10%, the electrical efficiency drops linearly from 13% to 9%. After that, the electrical efficiency hardly changes with the increasing shadow ratio. Dolara et al. conducted experiments on the c-Si PV module under partial shading conditions and reported that the effect of vertical shading on the PV module is consistent with the results of Wang et al. [27].

Table 5 Detailed results of I-V characteristics under different shaded areas.

	$A_{pv,s}/A_{pv}$ (%)	G (W/m^2)	U_{oc} (V)	I_{sc} (A)	U_{mp} (V)	I_{mp} (A)	P_{mp} (W)	η_{pv} (%)
Test 1	0	900.6	25.83	4.45	17.15	3.59	61.57	5.36
	8.3	901.0	25.67	3.96	17.73	3.16	56.03	5.31
	16.7	903.4	25.42	2.91	18.87	2.25	42.46	4.42
	25.0	904.8	24.99	1.63	19.87	1.21	24.04	2.78
Test 2	0	896.4	25.87	4.43	17.08	3.58	61.15	5.35
	8.3	897.8	25.73	3.99	17.73	3.16	56.03	5.33
	16.7	910.5	25.45	2.68	19.37	2.16	41.84	4.32
	25.0	915.4	24.96	1.48	20.44	1.13	23.10	2.64

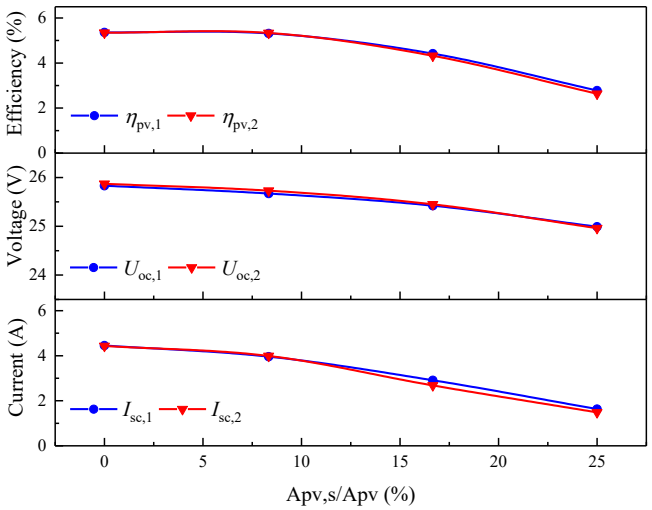

Fig. 13. Effect of the frame shadow on the performance of the a-Si-PV/T system.

3.2.2 Operating temperature

The operating temperature not only plays an important role in the thermal and electrical performance but also influences the light-induced degradation process of a-Si cells. The authors have conducted long-term experiments to investigate the effect of temperature on the a-Si-PV/T system and given the degradation of the electrical efficiency at 30 °C and 60 °C. Table 6 excerpts the results at 30 °C and 60 °C for ten days.

Table 6 Performance of a-Si-PV/T systems at 30 °C and 60 °C.

Date	t_d	$\overline{T_a}$(°C)	H(MJ/m^2)	$\eta_{th,a}$(%)		$\eta_{pv,a}$(%)		$\eta_{pvt,a}$(%)	
				30 °C	60 °C	30 °C	60 °C	30 °C	60 °C
2017.12.25	1	10.2	12.80	32.05	16.47	6.15	5.69	43.20	26.78
2018.01.12	6	2.6	14.48	29.64	15.08	5.97	5.52	40.45	25.09
2018.03.23	12	19.7	16.23	38.93	30.36	5.85	5.40	49.53	40.16
2018.04.17	18	21.9	16.14	41.74	29.26	5.84	5.44	52.33	39.11
2018.06.11	24	35.0	14.91	42.51	29.15	5.69	5.46	52.83	39.05
2018.10.31	30	21.7	13.20	38.17	21.53	5.55	5.39	48.26	31.30
2018.11.25	36	17.7	11.13	31.62	13.61	5.28	5.21	41.18	23.06
2019.04.15	42	20.6	14.02	38.04	25.31	5.55	5.44	48.09	35.18
2019.05.22	48	29.8	15.71	37.54	27.31	5.47	5.36	47.46	37.03
2019.06.12	54	30.3	13.45	37.11	26.91	5.51	5.32	47.10	36.55

According to the variation of the electrical efficiency in long-term experiments at 30 °C and 60 °C,

the formula of the electrical efficiency considered the operating temperature and time is fitted as follow:

$$\eta_{\mathrm{pv,mod}}=\eta_{\mathrm{pv}}\left[1-0.0009\left(423.15-T_{\mathrm{pv}}\right)\tanh\left(0.038t_{\mathrm{d}}\right)\right]. \quad (1)$$

Thus, the formula of the electrical gain is amended as:

$$E_{\mathrm{pv}}=G\tau_{\mathrm{g}}\tau_{\mathrm{ad}}\eta_{\mathrm{ref}}\left[1-B\left(T_{\mathrm{pv}}-T_{\mathrm{ref}}\right)\right]\left[1-0.0009\left(423.15-T_{\mathrm{pv}}\right)\tanh\left(0.038t_{\mathrm{d}}\right)\right]. \quad (2)$$

As shown in Fig. 14, the fitted curves of the electrical efficiency at 35 °C, 45 °C, and 55 °C are also presented. According to the fitted curves, the annual performance is analyzed at different operating temperatures. The system operated at these temperatures can be used for radiant floor heating in winter [31, 32].

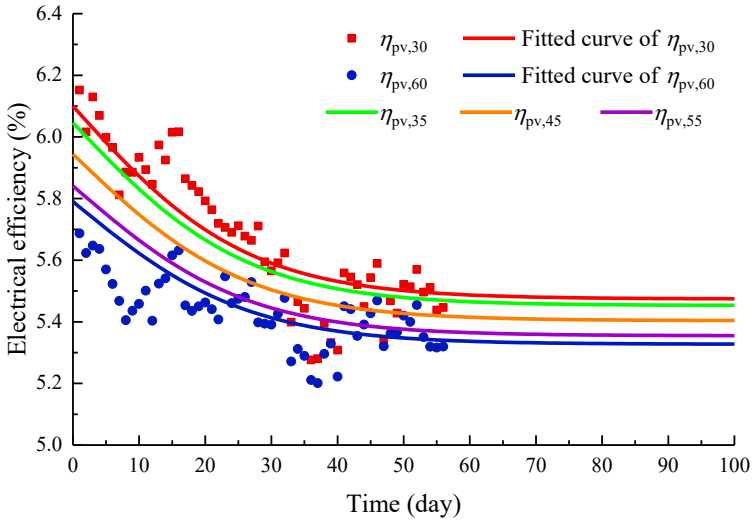

Fig. 14. Fitted curve of the electrical efficiency at 35 °C, 45 °C, and 55 °C.

The annual analysis is based on the meteorological data of a typical meteorological year from the EnergyPlus [33]. The a-Si-PV/T system runs daily from 8:00 to 16:00 in Hefei. The monthly meteorological data are shown in Fig. 15. The annual total solar irradiance is 3793.22 MJ/m^2. The annual average ambient temperatures of Hefei are above 0 °C, and the highest and lowest temperatures in July and January are 28.7 °C and 3.0 °C, respectively.

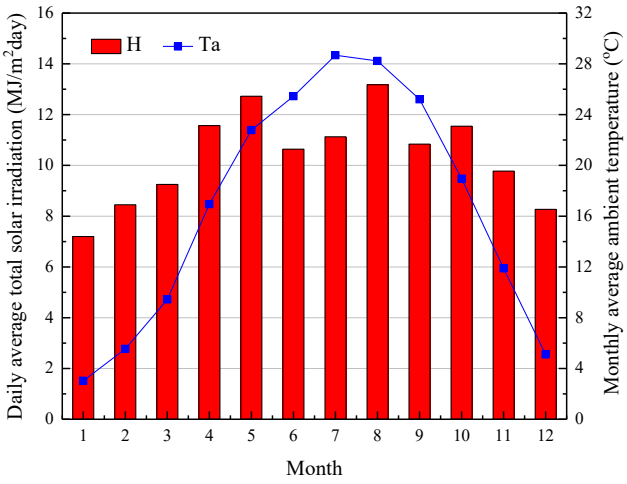

Fig. 15. Monthly average total solar irradiance and ambient temperature.

As shown in Fig. 16, the amounts of heat gain and electrical gain mainly depend on local solar irradiance. When the inlet temperatures are 35 °C, 45 °C, and 55 °C, the monthly heat gains range from 2.06 to 10.65 MJ/day, from 1.43 to 8.42 MJ/day, and from 0.94 to 6.25 MJ/day, respectively. In particular, the annual temperatures in Hefei are higher than 0 °C, thus this system is suitable for year-round operations. The effect of inlet temperature on electrical performance is less than that on thermal performance, and the electrical gain decreases marginally with increasing inlet temperature.

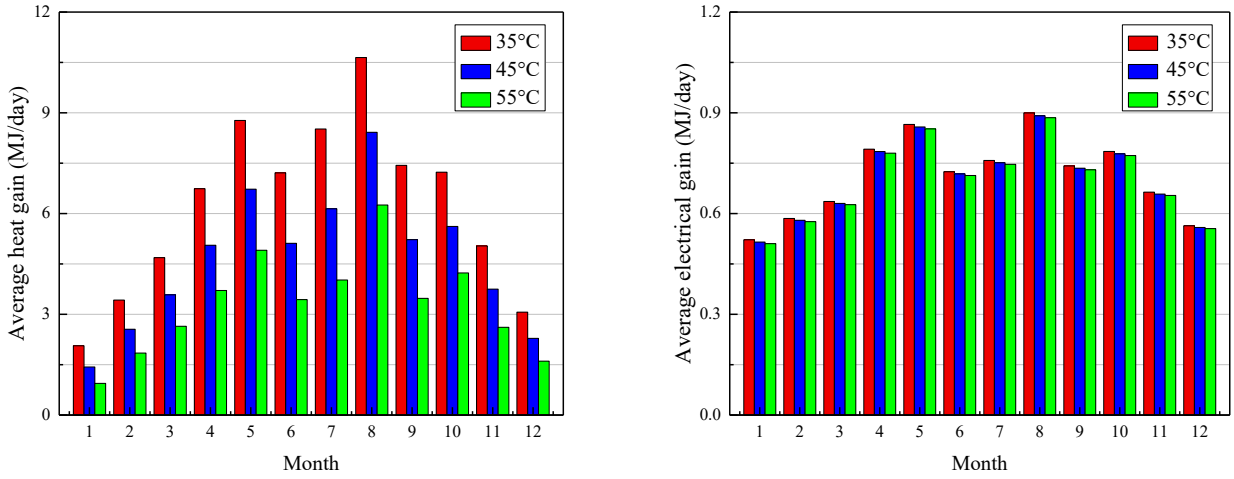

Fig. 16. Performance of the a-Si-PV/T system under different temperatures:
(a) Monthly heat gains; (b) Monthly electrical gains.

3.2.3 Mass flow rate of heat transfer fluid

In this section, the effect of the mass flow rate of heat transfer fluid and the temperature distribution

of the PV module and aluminum plate will be investigated in detail. The simulations are performed based on the DSS of a-Si cells and the parameters except mass flow rate are set as a fixed value, such as inlet temperature of 30 °C, ambient temperature of 10 °C, solar irradiance of 800 W/m^2, and wind velocity of 2 m/s. As shown in Fig. 17, the mass flow rate has a notable effect on both the thermal and electrical efficiency, especially at a low mass flow rate. However, as the mass flow rate increases, the overall exergy efficiency shows a declining trend, since the operating temperature drops. For instance, when the mass flow rate is 0.01 kg/s, the overall energy efficiency and exergy efficiency are about 45.49% and 7.12%, while the two values are 49.20% and 6.86% as the mass flow rate increases to 0.05 kg/s.

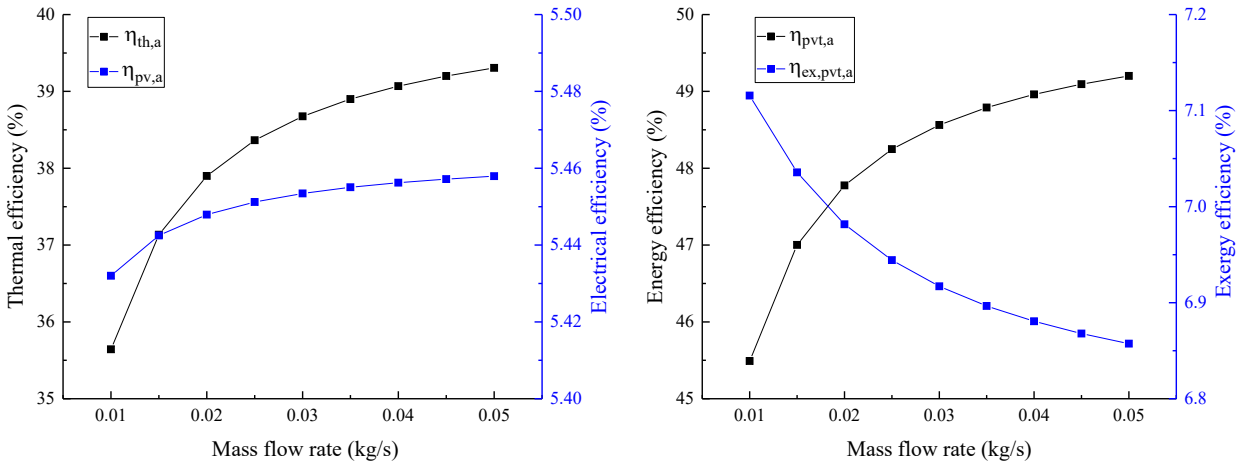

(a) (b)

Fig. 17. Effect of different mass flow rates on the performance of a-Si-PV/T system: (a) daily average thermal efficiency and electrical efficiency; (b) overall energy and exergy efficiency.

The temperature distributions under different mass flow rates of heat transfer fluid are presented in Fig. 18 and Fig. 19. With increasing mass flow rate, the temperature differences between the highest and lowest temperature of the PV module and absorber plate gradually decrease. For example, when the mass flow rate is 0.01 kg/s, the temperature difference of the absorber plate is 11.4 °C, while the value decreases to 3.2 °C with a mass flow rate of 0.05 kg/s. Moreover, as the mass flow rate increases

from 0.01 kg/s to 0.05 kg/s, the average temperatures of PV module and absorber plate decrease from 44.7 °C to 40.2 °C and from 43.8 °C to 39.3 °C.

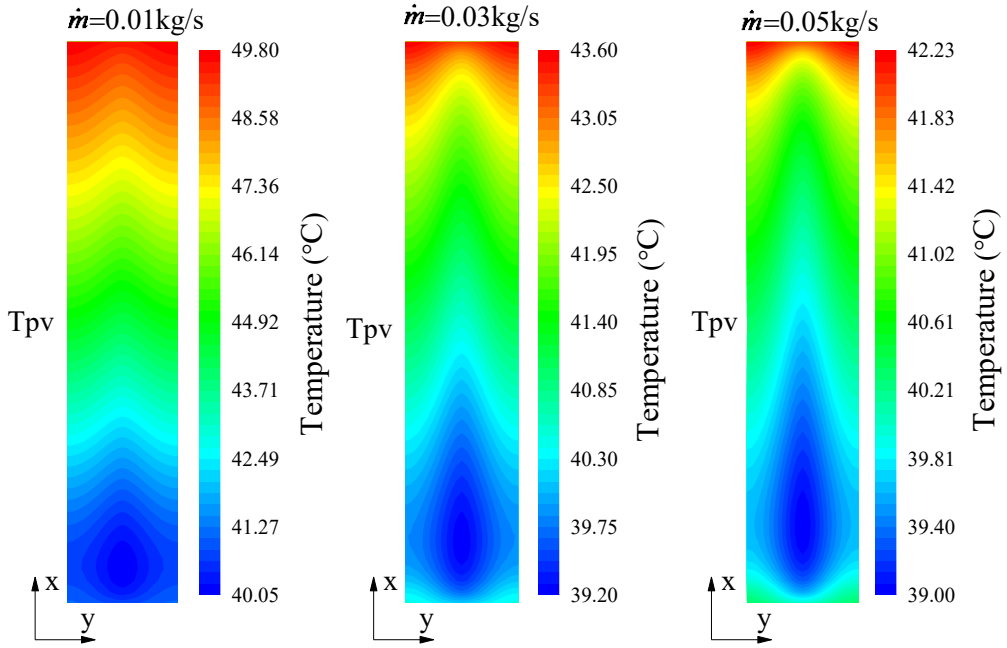

Fig. 18. Temperature distributions of the PV module at different mass flow rates.

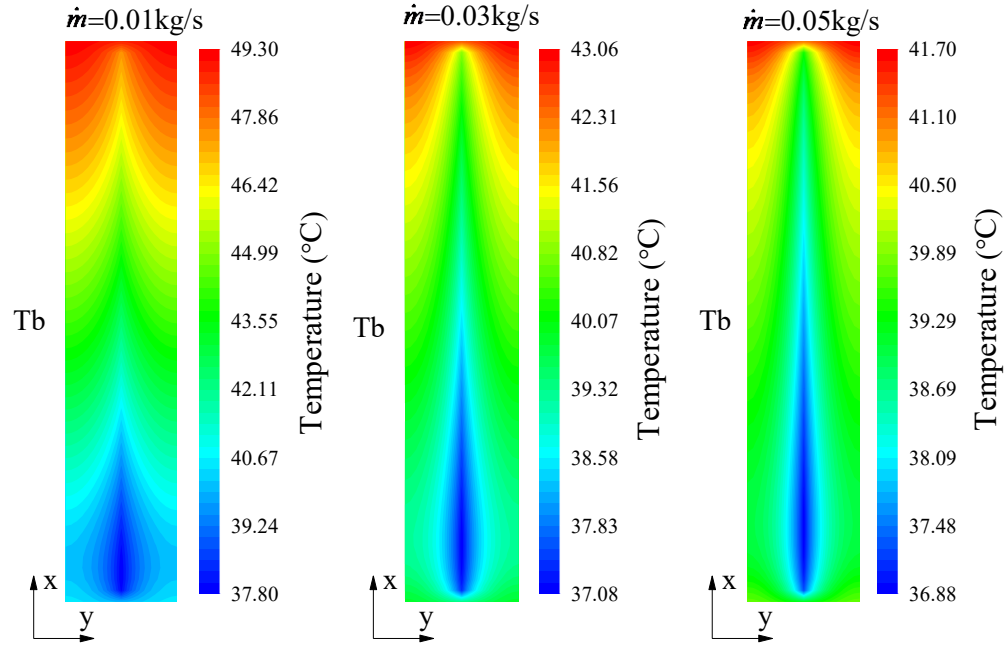

Fig. 19. Temperature distributions of the absorber plate at different mass flow rates.

3.2.4 Number of copper tubes

The number of copper tubes has a significant impact on the heat transfer of the a-Si-PV/T system.

The total mass flow rate of the system is set to a fixed value of 0.04 kg/s under different numbers of copper tubes. The simulation is based on the ambient temperature and solar irradiance on December 10 (Fig. 7) at DSS. As shown in Fig. 20, the number of copper tubes takes a significant positive connection with the final temperature of the water and the daily average thermal efficiency, but it has a slight effect on electrical efficiency. The thermal efficiency, overall energy efficiency and exergy efficiency have the same tendency: they all increase as the number of copper tubes increases, but the rate of growth gradually slows down. Specifically, when the number of copper tubes increases from 4 to 12, the daily average thermal efficiency enhances from 37.77% to 41.85%, and the daily average electrical efficiency rises from 5.42% to 5.45%. Therefore, considering the performance of the system and the manufacturing costs, seven or eight copper tubes are suitable for the a-Si-PV/T system.

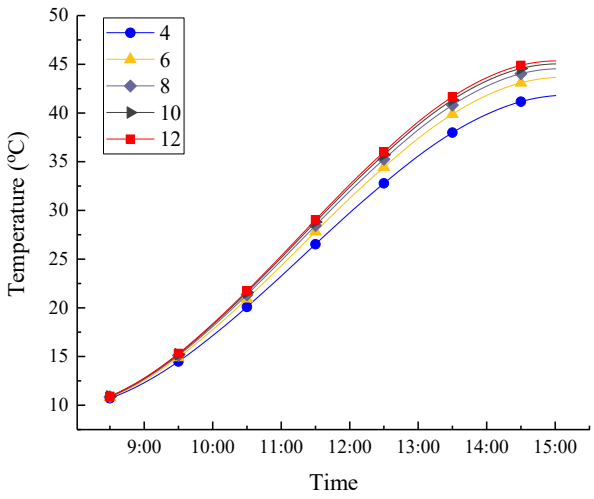

(a)

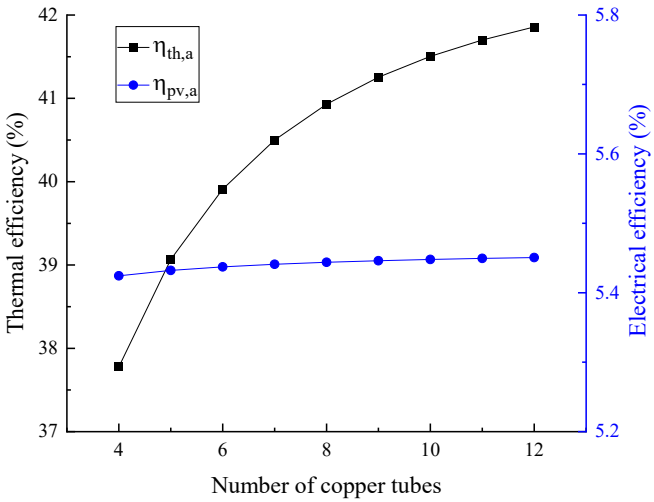

(b)

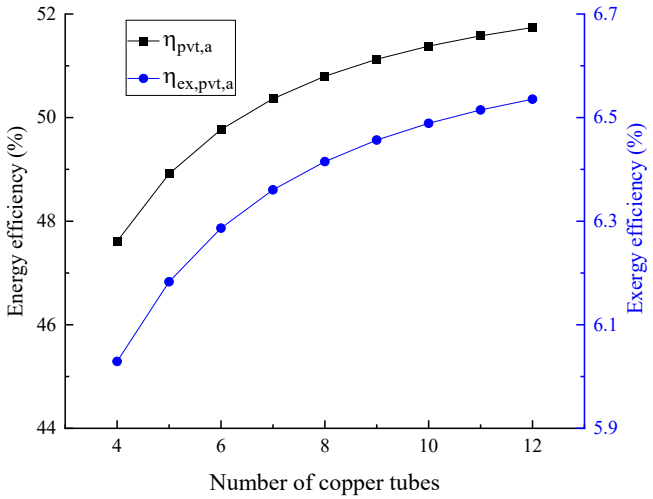

(c)

Fig. 20. Effect of different numbers of copper tubes on the performance of a-Si-PV/T system: (a) temperature of water in the tank; (b) daily average thermal efficiency and electrical efficiency; (c) overall energy and exergy efficiency.

The results in Fig. 21 and Fig. 22 are calculated on fixed values: inlet temperature of 30 °C, ambient temperature of 10 °C, solar irradiance of 800W/m^2, and wind velocity of 2 m/s. When the numbers of copper tubes are 4, 8, and 12, the average temperatures of the PV module are 45.8 °C, 39.6 °C, and 37.4 °C, and the values of the absorber plate are 44.9 °C, 38.7 °C, and 36.4 °C, respectively. The fewer the number of copper tubes, the higher the temperature of PV module and absorber plate. As can be seen from the temperature distribution, when the number of copper tubes is small, the heat absorbed by the absorber plate unconnected to the copper tube cannot be well utilized by the copper tube, which results in low thermal efficiency. Moreover, the temperature differences between the highest temperature and the lowest temperature of the PV module are 4.8 °C, 3.6 °C, and 3.5 °C, when the numbers are 4, 8, and 12. With the increase in the number of copper tubes, not only thermal efficiency increases but also the temperature distribution is more even.

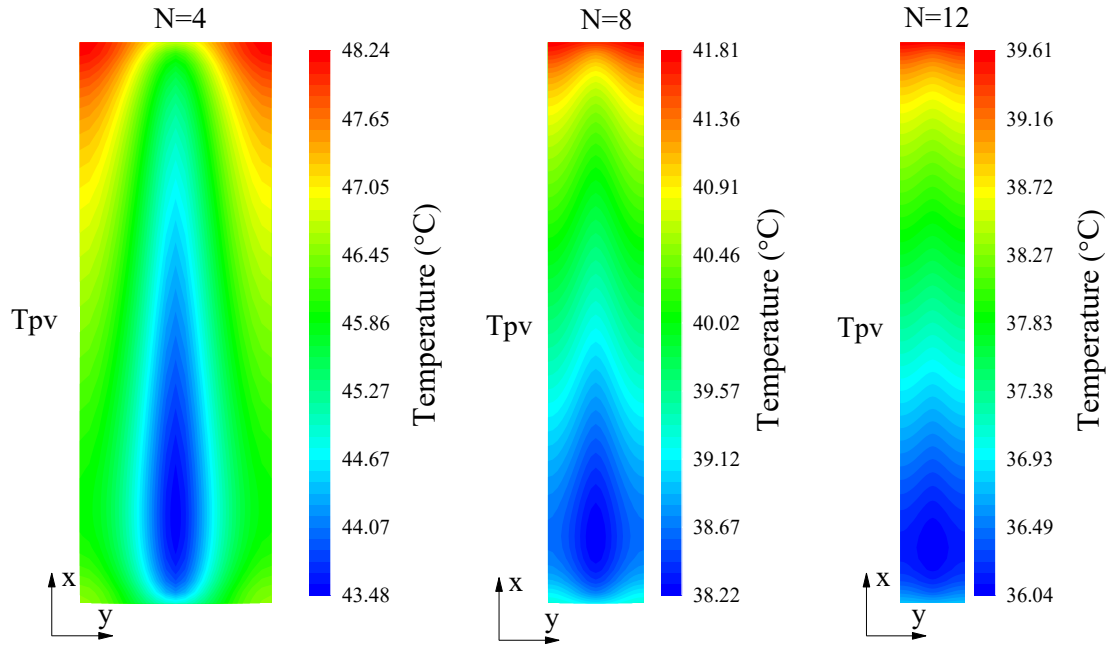

Fig. 21. Temperature distributions of the PV module at different numbers of copper tubes.

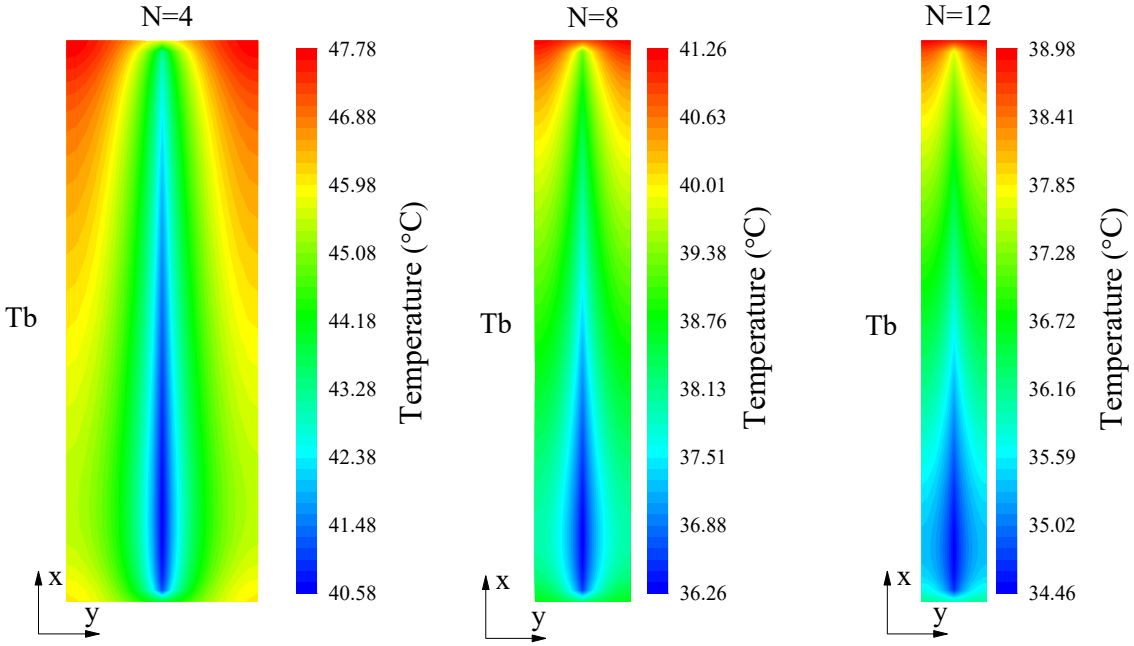

Fig. 22. Temperature distributions of the absorber plate at different numbers of copper tubes.

3.2.5 Cover ratio

To study the performance under different cover ratios, a simulation is carried out according to the mathematical model under the following fixed parameters: wind velocity of 2 m/s, mass flow rate of 0.04 kg/s, and absorber plate area of 1950 mm × 950 mm.

As shown in Fig. 23 (a), when the cover ratio increases from 0.01 to 0.99, the final temperature of the water drops from 51.1 °C to 41.1 °C. As shown in Fig. 23 (b), it is clear that the cover ratio shows a positive influence on electrical performance but a negative impact on thermal performance. As the cover ratio ascends from 0.01 to 0.99, the daily average electrical efficiency enhances from 5.41% to 5.46%, and the daily average thermal efficiency decreases from 48.58% to 36.95%. The larger the cover ratio, the larger the area of PV cells, which means that the more solar irradiance is obtained by the PV cells, and thus the greater the electrical gain. By contrast, with an increasing cover ratio, the solar irradiance received by the absorber plate correspondingly drops, resulting in a decrease in heat gain and daily thermal efficiency. As shown in Fig. 23(c), the calculation of the former takes into account the differences in the grades of thermal and electrical energy. When the cover ratio rises from 0.01 to 0.99, the overall energy efficiency and exergy efficiency increase from 48.72% to 51.17% and from 3.52% to 7.69%. This result indicates that the combination of the power generation and solar energy heating system can benefit the overall efficiency of solar energy harvesting.

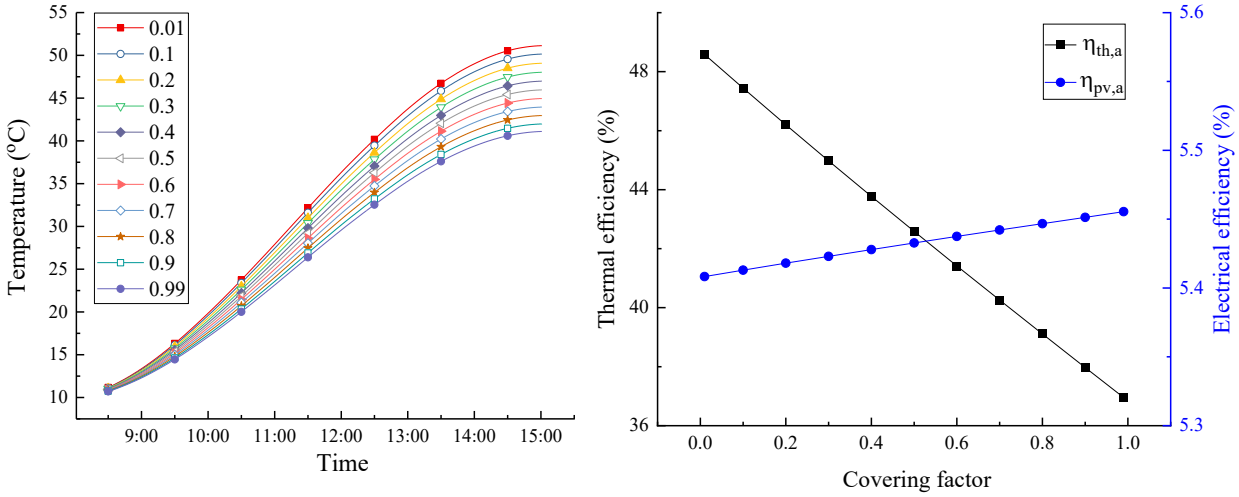

(a) (b)

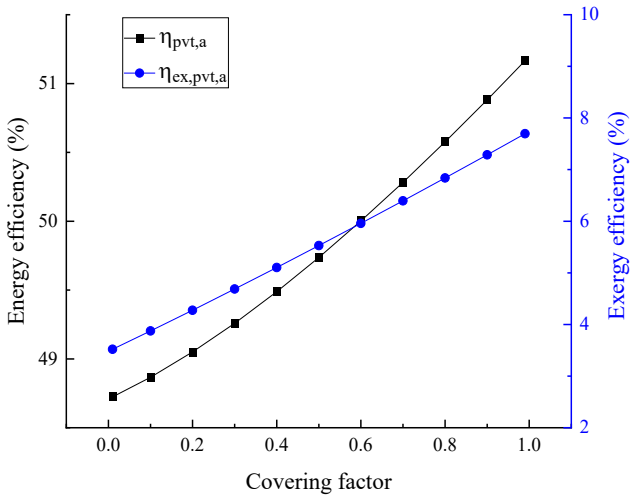

(c)

Fig. 23. Effect of different cover ratios on the performance of the a-Si-PV/T system: (a) temperature of water in the tank; (b) daily average thermal efficiency and electrical efficiency; (c) overall energy and exergy efficiency.

To investigate the temperature distributions at different cover ratios, parameters except cover ratio are set as a fixed value, such as inlet temperature of 30 °C, ambient temperature of 10 °C, solar irradiance of 800 W/m^2, and wind velocity of 2 m/s. The temperature distributions of the absorber plate with a cover ratio of 0.1, 0.5, and 0.9 are shown in Fig. 24. When the cover ratios are 0.1, 0.5, and 0.9, the average temperatures of the absorber plate are 41.0 °C, 39.6 °C, and 38.2 °C. According to Eq. (A16), the comprehensive absorption rate is the weighted average of black TPT and a-Si cells absorption rates, while the absorption of black TPT (0.95) is higher than that of a-Si cells (0.76). A higher cover ratio means a lower comprehensive absorption and represents a lower heat gain obtained by the absorber plate. Hence, as the cover ratio increases, the temperature of the absorber plate decreases, resulting in a decrease in thermal efficiency.

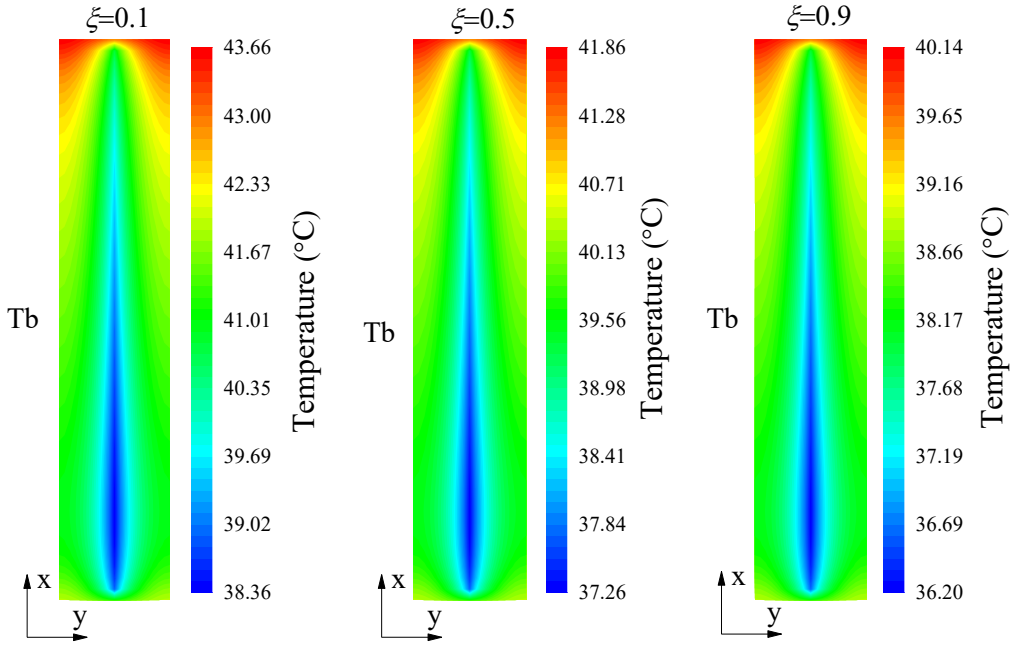

Fig. 24. Temperature distributions of the absorber plate at different cover ratios.

4. Conclusions

In this paper, the parametric analysis of thermodynamic parameters (operating temperature, mass flow rate), structure parameters (number of copper tubes, cover ratio), and frame shadow of the a-Si-PVT system are studied. A dynamic distributed parameter mathematical model is established and validated by outdoor experiments. Based on the verified model, parametric optimization and annual simulation are performed. The results are summarized as follows.

(1) The electrical performance at operating temperatures of 35 °C and 55 °C at the initial stage is about 6.05% and 5.84 % while it drops to 5.45% and 5.35% at DSS. The difference in electrical gain at different temperatures is significantly reduced at DSS. The mass flow rate applies a remarkable effect on both the thermal and electrical efficiency, especially at a low mass flow rate. The smaller the mass flow rate, the greater the temperature difference of the absorber plate (11.4 °C at a mass flow rate of 0.01 kg/s and 3.2 °C at 0.05 kg/s).

(2) An increment in the number of copper tubes applies a positive influence on thermal performance,

while an increment in the cover ratio exerts a negative effect on thermal performance. The influence of these parameters on electrical performance is minimal. Considering the overall efficiency and the manufacturing costs, this study finds that seven or eight copper tubes are suitable to achieve high overall efficiency. The overall exergy efficiency is positively associated with the number of copper tubes and cover ratio.

(3) When the shadow ratios are 0%, 8.3%, 16.7% and 25.0%, the electrical efficiencies each are 5.36%, 5.31%, 4.42% and 2.78%. As the shadow ratio ascends from 0 to 8.3%, it has little effect on electrical performance, but when it continues to increase, the electrical efficiency drops obviously. Moreover, the effect of frame shadow on the a-Si cells is different from that on the c-Si cells. To avoid a large shadow ratio during operation, the area of shadow ratio shall be less than 8.3%.

Acknowledgments

The study was sponsored by China Postdoctoral Science Foundation (2022M713463), National Natural Science Foundation of China (52206292), and the EU Marie Curie International Incoming Fellowships Program (703746), and the Major Program of the Natural Science Foundation of Shandong Province (No. ZR2019ZD11).

Appendix

The incident angle of solar irradiance on the surface of the collector is [34]

$$\begin{aligned}\cos\theta = {} & \sin\delta(\sin\phi\cos\beta - \cos\phi\sin\beta\cos\gamma) + \cos\delta\cos\omega\cos\phi\cos\beta \\ & + \cos\delta\cos\omega\sin\phi\sin\beta\cos\gamma + \cos\delta\sin\beta\sin\gamma\sin\omega\end{aligned}. \quad \text{(A1)}$$

Since the PV/T faces south, the incident angle is simplified as

$$\cos\theta = \sin\delta\sin(\phi-\beta) + \cos\delta\cos\omega\cos(\phi-\beta). \quad \text{(A2)}$$

For the glass cover, the energy balance equation is

$$\rho_g c_g d_g \frac{\partial T_g}{\partial t} = h_a \left(T_a - T_g\right) + h_{e,g} \left(T_e - T_g\right) + h_{g,pv} \left(T_{pv} - T_g\right) + G\alpha_g . \quad \text{(A3)}$$

The convective heat transfer coefficient between the glass cover and the surrounding air is given as

$$h_a = 2.8 + 3.0u_a . \quad \text{(A4)}$$

The sky temperature and the radiant heat transfer coefficient between the glass cover and sky are respectively given as

$$T_e = 0.0552T_a^{1.5}, \quad \text{(A5)}$$

$$h_{e,g} = \varepsilon_g \sigma (T_e^2 + T_g^2)(T_e + T_g) . \quad \text{(A6)}$$

The heat transfer coefficient between the glass cover and the PV cells combines radiation and convection is

$$h_{g,pv} = \sigma (T_{pv}^2 + T_g^2)(T_{pv} + T_g)\left(\frac{\xi}{1/\varepsilon_{pv} + \xi(1/\varepsilon_g - 1)} + \frac{1-\xi}{1/\varepsilon_{pv} + (1-\xi)(1/\varepsilon_g - 1)}\right) + \frac{Nu \cdot \lambda_a}{d_a} . \quad \text{(A7)}$$

The cover ratio of PV cells is

$$\xi = A_{pv} / A_c . \quad \text{(A8)}$$

And the Nusselt number is

$$Nu = 1 + 1.44\left(1 - \frac{1708(\sin 1.8\beta)^{1.6}}{Ra \cdot \cos\beta}\right)\left[1 - \frac{1708}{Ra \cdot \cos\beta}\right]^+ + \left[\left(\frac{Ra \cdot \cos\beta}{5830}\right)^{1/3} - 1\right]^+ , \quad \text{(A9)}$$

where $[]^+$ indicates that only positive values for the terms in the square brackets are used; in case of negative values, zero is used.

When the reflection is not considered, the transmittance of solar irradiance to the glass cover is

$$\tau_\alpha = e^{-KL} , \quad \text{(A10)}$$

$$L = d_g \Big/ \sqrt{1 - \left(\sin\theta / n_g\right)^2} \quad \text{(A11)}$$

The absorption of the glass cover is

$$\alpha_{\mathrm{g}} = 1 - \tau_{\alpha}. \tag{A12}$$

For the PV cells, the two-dimensional energy balance equation is

$$\rho_{\mathrm{pv}} c_{\mathrm{pv}} d_{\mathrm{pv}} \frac{\partial T_{\mathrm{pv}}}{\partial t} = \lambda_{\mathrm{pv}} d_{\mathrm{pv}} \left(\frac{\partial^2 T_{\mathrm{pv}}}{\partial x^2} + \frac{\partial^2 T_{\mathrm{pv}}}{\partial y^2} \right) + h_{\mathrm{g,pv}} \left(T_{\mathrm{g}} - T_{\mathrm{pv}} \right) + \left(T_{\mathrm{b}} - T_{\mathrm{pv}} \right) / R_{\mathrm{b,pv}} + G \left(\tau\alpha \right)_{\mathrm{pv}} - \xi P_{\mathrm{pv}}. \tag{A13}$$

The effective absorption $(\tau\alpha)_{\mathrm{pv}}$ and output power P_{pv} (W/m^2) of the PV cells are

$$\left(\tau\alpha \right)_{\mathrm{pv}} = \frac{\tau_{\mathrm{g}} \tau_{\mathrm{ad}} \alpha}{1 - \left(1 - \alpha \right) \rho_{\mathrm{d}}}, \tag{A14}$$

$$P_{\mathrm{pv}} = G \tau_{\mathrm{g}} \tau_{\mathrm{ad}} \eta_{\mathrm{ref}} \left[1 - B \left(T_{\mathrm{pv}} - T_{\mathrm{ref}} \right) \right] \left[1 - 0.0009 \left(423.15 - T_{\mathrm{pv}} \right) \tanh \left(0.038 t_{\mathrm{d}} \right) \right] \tag{A15}$$

The comprehensive absorption rate α is the weighted average of the values of black TPT (α_{TPT}) and PV module (α_{pv}) and given as

$$\alpha = \xi \alpha_{\mathrm{pv}} + \left(1 - \xi \right) \alpha_{\mathrm{TPT}}. \tag{A16}$$

The thermal resistance of the adhesive layer between the PV module and absorber plate is

$$R_{\mathrm{b,pv}} = \frac{d_{\mathrm{ad}}}{\lambda_{\mathrm{ad}}}. \tag{A17}$$

The energy balance equation of the absorber plate welded with the copper tubes is

$$\rho_{\mathrm{b}} c_{\mathrm{b}} d_{\mathrm{b}} \frac{\partial T_{\mathrm{b}}}{\partial t} = \lambda_{\mathrm{b}} d_{\mathrm{b}} \left(\frac{\partial^2 T_{\mathrm{b}}}{\partial x^2} + \frac{\partial^2 T_{\mathrm{b}}}{\partial y^2} \right) + \left(T_{\mathrm{pv}} - T_{\mathrm{b}} \right) / R_{\mathrm{b,pv}} + \frac{T_{\mathrm{t}} - T_{\mathrm{b}}}{R_{\mathrm{b,t}} \cdot A_{ij}}, \tag{A18}$$

where A_{ij} is the area of a single controller (m^2).

The energy balance equation of the other parts of the absorber plate is expressed as

$$\rho_{\mathrm{b}} c_{\mathrm{b}} d_{\mathrm{b}} \frac{\partial T_{\mathrm{b}}}{\partial t} = \lambda_{\mathrm{b}} d_{\mathrm{b}} \left(\frac{\partial^2 T_{\mathrm{b}}}{\partial x^2} + \frac{\partial^2 T_{\mathrm{b}}}{\partial y^2} \right) + \left(T_{\mathrm{pv}} - T_{\mathrm{b}} \right) / R_{\mathrm{b,pv}} + \left(T_{\mathrm{a}} - T_{\mathrm{b}} \right) / R_{\mathrm{b,a}}. \tag{A19}$$

The thermal resistance between the absorber plate and ambient air is

$$R_{\mathrm{b,a}} = d_{\mathrm{il}} / \lambda_{\mathrm{il}} + 1 / h_{\mathrm{a}}. \tag{A20}$$

The thermal resistance $R_{\mathrm{b,t}}$ between the absorber plate and the copper pipe is

$$R_{\mathrm{b,t}} = d_{\mathrm{bt}} \big/ \left(\lambda_{\mathrm{bt}} \cdot A_{\mathrm{bt}} \right), \tag{A21}$$

where A_{bt} is the welding area in a single controller (m^2).

For the copper tube, the energy balance equation is

$$A_{\mathrm{t}} \rho_{\mathrm{t}} c_{\mathrm{t}} \frac{\partial T_{\mathrm{t}}}{\partial t} = A_{\mathrm{t}} \lambda_{\mathrm{t}} \frac{\partial^2 T_{\mathrm{t}}}{\partial x^2} + \pi D_{\mathrm{t}} h_{\mathrm{w,t}} \left(T_{\mathrm{w}} - T_{\mathrm{t}} \right) + \frac{T_{\mathrm{b}} - T_{\mathrm{t}}}{R_{\mathrm{b,t}} \cdot dx}, \tag{A22}$$

where $h_{\mathrm{w,t}}$ is the convective heat transfer coefficient between the copper tube and the water flow ($\mathrm{W/(m^2 \cdot K)}$).

For the water flowing in the copper tube, the energy balance equation is

$$A_{\mathrm{w}} \rho_{\mathrm{w}} c_{\mathrm{w}} \frac{\partial T_{\mathrm{w}}}{\partial t} = -mc_{\mathrm{w}} \frac{\partial T_{\mathrm{w}}}{\partial x} + A_{\mathrm{w}} \lambda_{\mathrm{w}} \frac{\partial^2 T_{\mathrm{w}}}{\partial x^2} + C_{\mathrm{w}} h_{\mathrm{w,t}} \left(T_{\mathrm{t}} - T_{\mathrm{w}} \right), \tag{A23}$$

where $\dot{m}$ is the mass flow rate of the water in copper tubes (kg/s).

For the water in the water-storage tank, the energy balance equation is

$$A_{\mathrm{tank}} \rho_{\mathrm{w}} c_{\mathrm{w}} \frac{\partial T_{\mathrm{wt}}}{\partial t} = -mc_{\mathrm{w}} \frac{\partial T_{\mathrm{wT}}}{\partial x} + A_{\mathrm{tank}} \lambda_{\mathrm{w}} \frac{\partial^2 T_{\mathrm{wt}}}{\partial x^2} + C_{\mathrm{tank}} h_{\mathrm{tank}} \left(T_{\mathrm{a}} - T_{\mathrm{wt}} \right), \tag{A24}$$

where $\dot{M}$ is the mass flow rate of the water in water-storage tank (kg/s) and h_{tank} is the heat transfer coefficient between the water tank and the surrounding air ($\mathrm{W/(m^2 \cdot K)}$).

The instantaneous thermal efficiency can be defined as the heat gain between the outlet and inlet of the collector divided by the collector area and incident solar irradiance, expressed as:

$$\eta_{\mathrm{th}} = \frac{c_{\mathrm{w}} M \left(T_{\mathrm{out}} - T_{\mathrm{in}} \right)}{G A_{\mathrm{c}}}. \tag{A25}$$

The instantaneous electrical efficiency is given by:

$$\eta_{\mathrm{pv}} = \frac{P_{\mathrm{pv}}}{G A_{\mathrm{pv}}}. \tag{A26}$$

For the experimental electrical power is expressed as:

$$P_{\mathrm{pv}} = U_{\mathrm{mp}} I_{\mathrm{mp}}. \tag{A27}$$

As a widely accepted equation, the electrical efficiency is calculated by:

$$\eta_{\mathrm{pv}} = \eta_{\mathrm{ref}}\left[1 - B\left(T_{\mathrm{pv}} - T_{\mathrm{ref}}\right)\right]. \tag{A28}$$

When it comes to the a-Si-PV/T system, Eq.(A28) can not reflect the Staebler–Wronski Effect in the long term operation. The Staebler–Wronski Effect refers to metastable changes in a-Si cells properties caused by light-induced. It leads to a rapid decrease in electrical efficiency in the first several months. The SWE is complex and so far the mathematical model is lacked. As a first attempt, a hyperbolic tangent function (tanh) is employed in the paper to approximate this effect. Hyperbolic functions occur in the solutions of many linear differential equations (e.g. Laplace's equations) that are important in areas of physics, including heat transfer and fluid dynamics. The electrical efficiency is therefore calculated by:

$$\eta_{\mathrm{pv,mod}} = \eta_{\mathrm{pv}}\left[1 - c_1\left(423.15 - T_{\mathrm{pv}}\right)\tanh\left(c_2 t_{\mathrm{d}}\right)\right]. \tag{A29}$$

The items on the right of η_{pv} represent the electrical efficiency before the Staebler–Wronski Effect. t_{d} is the period of operation. 423.15 is the absolute temperature. On heating a-Si cells to above 423.15K (i.e., 150 °C), the Staebler–Wronski Effect can be reversed [35]. c_1 and c_2 are the coefficients to be determined by long term experiments, which is discussed in Section 4.1.1. A higher t_{d} leads to a lower electrical efficiency at a given operating temperature, but the decrement becomes less appreciable as t_{d} increases. Meanwhile, a higher T_{pv} can reduce the Staebler–Wronski Effect. Eq.(A29) can describe the nature of degradation dynamics of a-Si cells.

Since the shaded solar cells do not absorb solar energy or generate electricity, the effective power generation area of the solar cells is used when calculating the electrical efficiency. The electrical efficiency under different shaded areas is calculated by:

$$\eta_{\mathrm{pv}}=\frac{P_{\mathrm{pv}}}{G\left(A_{\mathrm{pv}}-A_{\mathrm{pv,s}}\right)}, \tag{A30}$$

where the A_{pv} and $A_{\mathrm{pv,s}}$ are the areas of the total PV module and the shadow (m^2).

The daily average thermal and electrical efficiencies are given as:

$$\eta_{\mathrm{th,a}}=\frac{Q_{\mathrm{th}}}{\int_{t_1}^{t_2}GA_{\mathrm{c}}dt}=\frac{c_{\mathrm{w}}M\left(\overline{T_{\mathrm{w,f}}}-\overline{T_{\mathrm{w,i}}}\right)}{\int_{t_1}^{t_2}GA_{\mathrm{c}}dt}, \tag{A31}$$

$$\eta_{\mathrm{pv,a}}=\frac{\int_{t_1}^{t_2}P_{\mathrm{pv}}dt}{\int_{t_1}^{t_2}GA_{\mathrm{pv}}dt}, \tag{A32}$$

where $\overline{T_{\mathrm{w,f}}}$ and $\overline{T_{\mathrm{w,i}}}$ are the final and initial average temperature of the water in the tank (K).

Electric energy is higher grade energy than thermal energy, thus the comprehensive efficiency considering energy grades is calculated by [36]:

$$\eta_{\mathrm{pvt,a}}=\eta_{\mathrm{th,a}}+\xi\frac{\eta_{\mathrm{pv,a}}}{\eta_{\mathrm{power}}}, \tag{A33}$$

where η_{power} is the conversion factor for the thermal power plant from thermal energy to electrical energy, and its value can be taken as 38%.

The instantaneous exergy efficiencies regarding heat gain and electrical gain are defined as:

$$\eta_{\mathrm{ex,th}}=\frac{Ex_{\mathrm{th}}}{Ex_{\mathrm{G}}A_{\mathrm{c}}}=\frac{c_{\mathrm{w}}M\left(T_{\mathrm{out}}-T_{\mathrm{in}}\right)\left(1-T_{\mathrm{a}}/T_{\mathrm{m}}\right)}{Ex_{\mathrm{G}}A_{\mathrm{c}}}, \tag{A34}$$

$$\eta_{\mathrm{ex,pv}}=\frac{Ex_{\mathrm{pv}}}{Ex_{\mathrm{G}}A_{\mathrm{pv}}}=\frac{P_{\mathrm{pv}}}{Ex_{\mathrm{G}}A_{\mathrm{pv}}}, \tag{A35}$$

where the exergy content of the solar irradiance and the mean thermodynamic temperature are calculated by:

$$Ex_{\mathrm{G}}=G\left(1-\frac{T_{\mathrm{a}}}{T_{\mathrm{sun}}}\right), \tag{A36}$$

$$T_{\mathrm{m}}=\frac{T_{\mathrm{out}}-T_{\mathrm{in}}}{\ln\left(T_{\mathrm{out}}/T_{\mathrm{in}}\right)}, \tag{A37}$$

where T_{sun} =5760K is the apparent solar temperature.

The daily average exergy efficiency of the heat gain according to the inlet and outlet temperature is given as:

$$\eta_{\mathrm{ex,th,a}}=\frac{\int_{t_1}^{t_2}Ex_{\mathrm{th}}dt}{\int_{t_1}^{t_2}Ex_{\mathrm{G}}A_{\mathrm{c}}dt}. \tag{A38}$$

The daily average exergy efficiencies and the overall exergy efficiency of the system according to the temperature of water in the tank are given as:

$$\eta_{\mathrm{ex,th,a}}=\frac{\int_{t_1}^{t_2}Ex_{\mathrm{wt}}dt}{\int_{t_1}^{t_2}Ex_{\mathrm{G}}A_{\mathrm{c}}dt}=\frac{\int_{t_1}^{t_2}c_{\mathrm{w}}M\frac{\partial T_{\mathrm{wt}}}{\partial t}\left(1-T_{\mathrm{a}}/T_{\mathrm{wt}}\right)dt}{\int_{t_1}^{t_2}Ex_{\mathrm{G}}A_{\mathrm{c}}dt}, \tag{A39}$$

$$\eta_{\mathrm{ex,pv,a}}=\frac{\int_{t_1}^{t_2}Ex_{\mathrm{pv}}dt}{\int_{t_1}^{t_2}Ex_{\mathrm{G}}A_{\mathrm{pv}}dt}, \tag{A40}$$

$$\eta_{\mathrm{ex,pvt,a}}=\eta_{\mathrm{ex,th,a}}+\xi\eta_{\mathrm{ex,pv,a}}. \tag{A41}$$

The calculation of uncertainty is given by

$$\frac{\Delta y}{y}=\left[\left(\frac{\partial f}{\partial x_1}\right)^2\left(\frac{\Delta x_1}{y}\right)^2+\left(\frac{\partial f}{\partial x_2}\right)^2\left(\frac{\Delta x_2}{y}\right)^2+\cdots+\left(\frac{\partial f}{\partial x_n}\right)^2\left(\frac{\Delta x_n}{y}\right)^2\right]^{\frac{1}{2}}, \tag{A42}$$

where f is the function of indirect measurement that requires an uncertainty analysis; x is one of the variables of the function; Δx is the absolute error of the variable.

To evaluate the consistency between the simulation and the experimental results, the relative error (RE) and mean relative error (MRE) are defined as

$$RE=\frac{X_{\mathrm{exp}}-X_{\mathrm{sim}}}{X_{\mathrm{exp}}}\times 100\%, \tag{A43}$$

$$MRE = \frac{\sum_{i=1}^{i=N} \left| X_{\text{exp}} - X_{\text{sim}} \right|}{\sum_{i=1}^{i=N} X_{\text{exp}}} \times 100\% , \tag{A44}$$

where X_{exp} and X_{sim} are the experimental and simulation results, respectively.

References

[1] Jie J, Gang P, Wei H, Wei S, Guiqiang L, Jing L. Research progress on solar photovoltaic/thermal systems utilization. Beijing: Science Press; 2017.

[2] Pathak MJM, Pearce JM, Harrison SJ. Effects on amorphous silicon photovoltaic performance from high-temperature annealing pulses in photovoltaic thermal hybrid devices. Solar Energy Materials and Solar Cells. 2012;100:199-203.

[3] Kutlu C, Li J, Su YH, Wang YB, Pei G, Riffat S. Investigation of an innovative PV/T-ORC system using amorphous silicon cells and evacuated flat plate solar collectors. Energy. 2020;203:117873.

[4] Platz R, Fischer D, Zufferey MA, Selvan JAA, Haller A, Shah A. Hybrid collectors using thin-film technology. Ieee Phot Spec Conf. 1997:1293-6.

[5] Köntges M, Kunze I, Kajari-Schröder S, Breitenmoser X, Bjørneklett B. The risk of power loss in crystalline silicon based photovoltaic modules due to micro-cracks. Solar Energy Materials and Solar Cells. 2011;95:1131-7.

[6] Jia R, Tao K, Li Q, Dai XW, Sun HC, Sun Y, et al. Influence of using amorphous silicon stack as front heterojunction structure on performance of interdigitated back contact-heterojunction solar cell (IBC-HJ). Front Energy. 2017;11:96-104.

[7] Mateo C, Hernández-Fenollosa MA, Montero Á, Seguí-Chilet S. Ageing and seasonal effects on amorphous silicon photovoltaic modules in a Mediterranean climate. Renewable Energy. 2022;186:74-

88.

[8] Virtuani A, Fanni L. Seasonal power fluctuations of amorphous silicon thin-film solar modules: distinguishing between different contributions. Progress in Photovoltaics: Research and Applications. 2014;22:208-17.

[9] Ruther R, Tamizh-Mani G, del Cueto J, Adelstein J, Dacoregio MM, von Roedern B. Performance test of amorphous silicon modules in different climates - Year three: Higher minimum operating temperatures lead to higher performance levels. Conference Record of the Thirty-First IEEE Photovoltaic Specialists Conference - 2005. 2005:1635-8.

[10] Huang MX, Wang YF, Li M, Keovisar V, Li XJ, Kong DC, et al. Comparative study on energy and exergy properties of solar photovoltaic/thermal air collector based on amorphous silicon cells. Applied Thermal Engineering. 2021;185:116376.

[11] Li J, Ren X, Yuan WQ, Li ZM, Pei G, Su YH, et al. Experimental study on a novel photovoltaic thermal system using amorphous silicon cells deposited on stainless steel. Energy. 2018;159:786-98.

[12] Ren X, Li J, Hu MK, Pei G, Jiao DS, Zhao XD, et al. Feasibility of an innovative amorphous silicon photovoltaic/thermal system for medium temperature applications. Applied Energy. 2019;252:113427.

[13] Amanlou Y, Hashjin TT, Ghobadian B, Najafi G. Air cooling low concentrated photovoltaic/thermal (LCPV/T) solar collector to approach uniform temperature distribution on the PV plate. Applied Thermal Engineering. 2018;141:413-21.

[14] Hossain MS, Pandey AK, Selvaraj J, Abd Rahim N, Rivai A, Tyagi VV. Thermal performance analysis of parallel serpentine flow based photovoltaic/thermal (PV/T) system under composite climate of Malaysia. Applied Thermal Engineering. 2019;153:861-71.

[15] Li ZM, Ji J, Yuan WQ, Song ZY, Ren X, Uddin MM, et al. Experimental and numerical investigations on the performance of a G-PV/T system comparing with A-PV/T system. Energy. 2020;194.

[16] Maadi SR, Khatibi M, Ebrahimnia-Bajestan E, Wood D. Coupled thermal-optical numerical modeling of PV/T module - Combining CFD approach and two-band radiation DO model. Energy Conversion and Management. 2019;198.

[17] Yu QW, Hu MK, Li JF, Wang YY, Pei G. Development of a 2D temperature-irradiance coupling model for performance characterizations of the flat-plate photovoltaic/thermal (PV/T) collector. Renewable Energy. 2020;153:404-19.

[18] Pathak MJM, Girotra K, Harrison SJ, Pearce JM. The effect of hybrid photovoltaic thermal device operating conditions on intrinsic layer thickness optimization of hydrogenated amorphous silicon solar cells. Solar Energy. 2012;86:2673-7.

[19] Rozario J, Vora AH, Debnath SK, Pathak MJM, Pearce JM. The effects of dispatch strategy on electrical performance of amorphous silicon-based solar photovoltaic-thermal systems. Renewable Energy. 2014;68:459-65.

[20] Frigeri C, Serényi M, Szekrényes Z, Kamarás K, Csik A, Khánh NQ. Effect of heat treatments on the properties of hydrogenated amorphous silicon for PV and PVT applications. Solar Energy. 2015;119:225-32.

[21] Xie M, Ren CR, Fu LM, Qiu XD, Yu XG, Yang DR. An industrial solution to light-induced degradation of crystalline silicon solar cells. Front Energy. 2017;11:67-71.

[22] Kichou S, Silvestre S, Nofuentes G, Torres-Ramirez M, Chouder A, Guasch D. Characterization of degradation and evaluation of model parameters of amorphous silicon photovoltaic modules under

outdoor long term exposure. Energy. 2016;96:231-41.

[23] Ishii T, Otani K, Takashima T, Ikeda K. Change in I-V characteristics of thin-film photovoltaic (PV) modules induced by light soaking and thermal annealing effects. Prog Photovoltaics. 2014;22:949-57.

[24] Li ZM, Ji J, Yuan WQ, Zhao B, Zhou F, Uddin MM, et al. Experimental & numerical investigation and optimization on a novel flat-plate PV/T system using CdfTe thin-film solar modules of sandwich structure. Solar Energy. 2021;223:261-77.

[25] Bressan M, Gutierrez A, Garcia Gutierrez L, Alonso C. Development of a real-time hot-spot prevention using an emulator of partially shaded PV systems. Renewable Energy. 2018;127:334-43.

[26] Wang YY, Pei G, Zhang LC. Effects of frame shadow on the PV character of a photovoltaic/thermal system. Applied Energy. 2014;130:326-32.

[27] Dolara A, Lazaroiu GC, Leva S, Manzolini G. Experimental investigation of partial shading scenarios on PV (photovoltaic) modules. Energy. 2013;55:466-75.

[28] Wang YY, Ke SM, Liu FS, Li JF, Pei G. Performance of a building-integrated photovoltaic/thermal system under frame shadows. Energy and Buildings. 2017;134:71-9.

[29] Malathy S, Ramaprabha R. Comprehensive analysis on the role of array size and configuration on energy yield of photovoltaic systems under shaded conditions. Renew Sust Energ Rev. 2015;49:672-9.

[30] Kesler S, Kivrak S, Gurleyen H, Dincer F, Yilmaz S, Ozcalik HR. A Low Cost Shading Analyzer and Site Evaluator Design to Determine Solar Power System Installation Area. International Journal of Photoenergy. 2015;2015.

[31] Sattari S, Farhanieh B. A parametric study on radiant floor heating system performance.

Renewable Energy. 2006;31:1617-26.

[32] Shin MS, Rhee KN, Ryu SR, Yeo MS, Kim KW. Design of radiant floor heating panel in view of floor surface temperatures. Build Environ. 2015;92:559-77.

[33] https://www.energyplus.net/weather.

[34] Duffie JA, Beckman WA. Solar Engineering of Thermal Processes, Fourth Edition: John Wiley & Sons Inc; 2013.

[35] Staebler DL, Wronski CR. Reversible Conductivity Changes in Discharge-Produced Amorphous Si. Applied Physics Letters. 1977;31:292-4.

[36] Ji J, Lu J-P, Chow T-T, He W, Pei G. A sensitivity study of a hybrid photovoltaic/thermal water-heating system with natural circulation. Applied Energy. 2007;84:222-37.